METEOROLOGICAL OFFICE
-1 AUG 1980
LIBRARY

132918

Met O 11 Technical Note No 139

Progress report on models with alternative mechanisms of geostrophic adjustment

by

M J P Cullen

Met O 11
Meteorological Office
London Road
Bracknell
Berkshire

July 1980

NOTE: This paper has not been published. Permission to quote from it must be obtained from the Assistant Director of the above Meteorological Office branch.

DH

1. Introduction

This note describes current progress on models designed to study alternative representations of the geostrophic adjustment process in the atmosphere. It is an updated version of MRCP 464 (Cullen (1979)) and contains a considerable amount of material from the MRCP which only had a limited distribution. This work is still not at a definitive stage and this note therefore includes ideas which are not yet validated and are the subject of current research, as well as ideas which have been more fully worked out.

This work is motivated by the apparent convergence of numerical forecasting results with increased resolution and complexity of formulation to a standard which is useful but falls well short of expectations from predictability studies. This is most conveniently illustrated by graphs of rms error growth (eg Kasahara (1979)) but is also supported by several model intercomparison studies (Baumhefner and Downey (1978), Cullen et al (1981), Findlater (1980), Gadd (1980)). These studies show rapid rms error growth in the first 12 hours of a forecast and marked insensitivity to changes in model formulation. Current work on developing the new Meteorological Office model has also shown a marked lack of sensitivity to the formulation. There are several possible explanations for this situation. The fundamental limit of prediction may have been reached, and the predictability studies may not have modelled the error growth correctly. Alternatively models may be as good as they can be but the initial conditions are deficient. This is almost certainly true to some extent but it is difficult to determine whether this explains all the errors. Otherwise there may be errors in the model formulation. Current experience suggests that the numerical solution of the primitive equations and the representation of physical processes are not the major course of forecasting errors, except on small scales, once the resolution reaches the level of the largest Meteorological Office models. It is therefore worth looking for deficiencies in the formulation at a more basic level.

This note proposes and investigates the following explanation for the major forecast errors. In middle and high latitudes the atmosphere is close to geostrophic balance. Given an initially geostrophic state, however, advection by the geostrophic wind will tend to destroy it and a secondary circulation has to be set up to maintain it; eg see Hoskins et al (1978). This is achieved because any departure from geostrophic balance sets up a divergence field which mutually adjusts the height and wind fields towards quasi-geostrophic balance. This adjustment mechanism assumes that gravity waves can be set up, a local excess of pressure not balanced by the Coriolis term will set up an outflow of air which reduces the excess and simultaneously affects the vertical component of the vorticity field through compression of the vortex filaments. It is possible to write equations which do not actually describe the gravity waves explicitly, but their presence is still assumed implicitly.

In middle and high latitudes the atmosphere is rotating rapidly in the sense that the Rossby number U/fL is less than 1 for synoptic scale features. Tropospheric motions are also constrained by the pressure of the strongly stably stratified layer above them, and by the bottom boundary. Under such circumstances overturning motions tend to be inhibited. Gravity waves are usually only to be observed in the neighbourhood of strong local discontinuities such as fronts or jet streams. As in some other fluid problems the motion tends to be smooth almost everywhere with strong vertical motions and overturning confined to small regions and near boundaries. In such regions the Rossby number can be large and quasi-geostrophic balance will not hold. In the stratosphere, however, where the flow is less constrained, large scale tidal waves are observed.

The primitive equations and filtered equations both assume that the quasi-geostrophic balance is maintained by the presence of the gravity wave mechanism on all horizontal and vertical scales. It is found that the resulting mutual adjustment of wind and height fields is scale dependent in a particular way (see next section and Blumen (1972)). If, however, the overturning motions

involved in adjustment can only take place in restricted regions, then this scale dependence may not be correct. A trivial example shows how large this effect could be. Consider a barotropic wave in geostrophic balance. The vorticity advection will tend to translate it at the Rossby wave speed; but the height advection will be zero since the wind blows along the contours. Therefore any speed between zero and the Rossby wave speed can be achieved by an appropriate adjustment mechanism.

In the next section of the note these ideas are set out mathematically. Finding an improved way of representing this adjustment is very difficult. Two approaches are discussed. The first attempts to modify the equations in the light of the proposed constraints on the motions. This has not yet been pursued very far. The second approach is to parametrize the process, in the same sense as convection and surface exchanges are already parametrized in models. To do this various gross properties of the adjustment process must be recognised, some possibilities are discussed.

The third section contains results from a search for empirical relationships between observed developments and geostrophic advection terms in the equations. This uses some relationships from descriptive forecasting rules and is helpful in constructing parametrization schemes. In the fourth section a particular scheme is described and results from it are shown. It should be emphasised that no scheme has yet been found which produces a better forecast than the normal equations.

2. The mathematical theory of geostrophic adjustment

2.1 The theory for the shallow water equations

As a first example, consider the shallow water equations on an f plane in vorticity and divergence form:

$$\begin{aligned} \frac{\partial \zeta}{\partial t} + \underline{u}.\nabla(\zeta+f) + (\zeta+f)D &= 0 \\ \frac{\partial D}{\partial t} + \nabla.(\underline{u}.\nabla\underline{u}) + \nabla^2\phi - f\zeta &= 0 \\ \frac{\partial \phi}{\partial t} + \underline{u}.\nabla\phi + \phi D &= 0 \end{aligned} \qquad (1)$$

Linearise these about a basic state given by

$$\phi = \bar{\Phi}(y) \quad , \quad \zeta = 0 \quad , \quad D = 0$$

$$\underline{u} = (U, 0) \qquad \text{with} \qquad f U = -\bar{\Phi}_y \quad , \quad \bar{\Phi}_{yy} = 0$$

Also assume $\bar{\Phi}(y) = \bar{\Phi}_0$ to first order

$$\begin{aligned} &\frac{\partial \zeta}{\partial t} + U\frac{\partial \zeta}{\partial x} + f D = 0 \\ &\frac{\partial D}{\partial t} + U\frac{\partial D}{\partial x} + \nabla^2\phi - f\zeta = 0 \\ &\frac{\partial \phi}{\partial t} + U\frac{\partial \phi}{\partial x} + v\bar{\Phi}_y + \bar{\Phi}_0 D = 0 \end{aligned} \qquad (2)$$

Seek normal mode solutions of (2) proportional to $e^{i(kx-\omega t)}$.

Then the normal mode condition is

$$\begin{vmatrix} -i\omega + ikU & f & 0 \\ -f & -i\omega + ikU & -k^2 \\ -fU/ik & \bar{\Phi}_0 & -i\omega + ikU \end{vmatrix} = 0$$

This reduces to

$$f^2\omega + (\omega - kU)(k^2\bar{\Phi}_0 - (\omega - kU)^2) = 0 \qquad (3)$$

In the case $U = 0$ the solutions are

$$\omega = 0, \quad \omega = \pm\sqrt{k^2\bar{\Phi}_0 + f^2} \qquad (4)$$

The zero solution corresponds to the geostrophic solution, the other solutions to gravity waves. In the general case (3), if $k^2\bar{\Phi}_0 \gg f^2$, the geostrophic solution tends to $\omega = kU$, if $f^2 \gg k^2\bar{\Phi}_0$ and k^2U^2, it tends to $\omega = 0$. This supports the statement in the introduction that by varying

the parameters controlling the mutual adjustment of wind and height fields, the speed of the meteorological wave can vary between 0 and U. The scale dependence calculated here shows that for large vertical and small horizontal scales, ($k^2 \underline{\Phi}_0$ large), heights adjust to the winds and vice versa.

2.2 The theory for a two layer model

A full normal mode analysis of a two level primitive equation model is set out in Foreman (1978), which is hereafter referred to as F. The analysis in F is carried out in sigma co-ordinates and leads to seven eigensolutions for a two layer model. The extra solution comes about because there are three variables controlling the height field, surface pressure and two temperatures; the geostrophic constraint will relate winds at the two levels to two special linear combinations of pressure and temperature. There will then be a redundant mode with no geopotential perturbation at either level. This mode will be weakly coupled into the system through the advection terms. The analysis in F is carried out for various basic state wind shears and has to be done numerically. To illustrate the behaviour the case of zero basic state wind on an f plane is set out here:

Equations 3.4.1 to 3.4.7 of F with $U=0$, $\beta=0$ become:

$$\frac{d}{k}(iv_n) = -f_0/k\, u_n \qquad (5.1,2)$$

$$\frac{d}{k} u_n = -f_0/k\, iv_n - \phi_n - \frac{R\bar{T}_{m,n} p_s}{p_0} \qquad (5.3,4)$$

$$\frac{d}{k} T_n = i\frac{\sigma \delta_\sigma \bar{T}_{m,n}^{\sigma}}{k} + \frac{i\kappa \bar{T}_{m,n}\omega_n}{k p_0 \sigma} \qquad (5.5,6)$$

$$\frac{d}{k} p_s = -p_0 (u_1 + u_2)\Delta\sigma \qquad (5.7)$$

where

$$\phi_2 = R\bar{T}_2 \ln 1/\sigma_2 \qquad \phi_1 = \phi_2 + \tfrac{1}{2} R(\bar{T}_1 + \bar{T}_2) \ln \sigma_2/\sigma_1$$

$$p_0 \dot{\sigma}_{1\frac{1}{2}} = ik\sigma_{1\frac{1}{2}} p_0 (u_1 + u_2)\Delta\sigma - ik p_0 u_1 \Delta\sigma \,, \quad \dot{\sigma}_{2\frac{1}{2}} = \dot{\sigma}_{\frac{1}{2}} = 0$$

$$-\left(\frac{\kappa \bar{T}_m \omega}{p_0 \sigma}\right)_n = -ik\kappa \bar{T}_{m,n} \left(\tfrac{1}{2} \ln \frac{\sigma_{n+1}}{\sigma_n} \sum_{s=1}^{n} u_s + \tfrac{1}{2} \ln \frac{\sigma_n}{\sigma_{n-1}} \sum_{s=1}^{n-1} u_s \right)$$

Since the right hand sides of 5.5,5.6 and 5.7 only involve u_1 and u_2, 5.1 and 5.2 can be used to construct three zero solutions for α/k. Writing the equations in matrix form, the normal mode condition can be reduced to

$$\begin{vmatrix} -f_0/k + \alpha^2/f_0 k & 0 & -R d_0 & -R d_1 & -\frac{RT_{m_1}}{p_0} \\ 0 & f_0/k + \alpha^2/f_0 k & 0 & -R d_2 & -\frac{RT_{m_2}}{p_0} \\ A_{11} & A_{12} & -1/k & 0 & 0 \\ A_{21} & A_{22} & 0 & -1/k & 0 \\ p_0/2f_0 & p_0/2f_0 & 0 & 0 & -1/k \end{vmatrix} = 0 \qquad (6)$$

where we have taken $\sigma_1 = 1/4$, $\sigma_2 = 3/4$ and defined

$$d_0 = \tfrac{1}{2}\ln 3, \quad d_1 = \tfrac{1}{2}\ln 3 + \ln 4/3, \quad d_2 = \ln 4/3,$$

$$A_{11} = -\tfrac{1}{f_0}\left(\tfrac{1}{4}(T_{m2} - T_{m1}) + \kappa T_{m1} d_0\right), \quad A_{12} = \frac{1}{4f_0}(T_{m2} - T_{m1}),$$

$$A_{21} = -\tfrac{1}{f_0}\left(\tfrac{1}{4}(T_{m2} - T_{m1}) + \kappa T_{m2} d_1\right), \quad A_{22} = -\tfrac{1}{f_0}\left(-\tfrac{1}{4}(T_{m2} - T_{m1}) + \kappa d_2 T_{m2}\right)$$

(6) has two solutions for α^2, corresponding to two pairs of gravity waves with solutions of the form $\alpha = \pm k\sqrt{\Phi_i}$ where the Φ_i are equivalent depths like the Φ_0 of section 2.1. It is easier to derive the full solution in the absence of the rotation terms. In this case (6) reduces to the eigensolution condition for pure gravity waves. Such a solution is described for a 5 level model in Hoskins and Simmons (1975). There are 5 equivalent depths, the largest is about 10^5 $m^2 s^{-2}$ and the smallest about 20 $m^2 s^{-2}$. The eigenfunction associated with the largest equivalent depth is of constant sign with height, while the others have successively more changes of sign. For the two level case values of Φ_0 would be about 10^5 and 10^4 with eigenfunctions roughly like (1,1) and(1,-1) respectively.

Now consider the case where there is a basic state wind. In the one level case vorticity advection implies that a quasi geostrophic disturbance propagates at a speed U, while height advection implies that it is stationary. In the two level case the inconsistency between the two advection effects is much

more complicated if the basic state wind has vertical shear. The relative adjustment of the two fields will depend on whether the imbalances generated by advection are of the same or opposite signs at the two levels and which type of gravity wave is generated. In order to obtain a quasi geostrophic normal mode the divergence must balance the disruptive effect of the vertical shear as well as maintaining quasi geostrophic balance. It is found that in the resulting quasi geostrophic modes the divergence is of the same order of magnitude as the vorticity and that neutral solutions can often not be obtained for the quasi geostrophic modes but an exponential pair is obtained. A large number of such solutions are set out in [-] . This is regarded as indicating baroclinic instability of the basic state. It is clear that the structures of the quasi geostrophic modes are intimately related to the presence in the equations of terms describing the gravity waves. If these waves cannot occur in reality except in limited regions, then the nature of the allowed quasi geostrophic modes will be different from those derived from the primitive equations. In a forecast using the primitive equations there would then be an initial period of adjustment while the model extracted the quasi geostrophic primitive equation normal modes from the initial data. The same applies if filtered equations are used because these are designed to have the same quasi geostrophic modes as the primitive equations.

2.3 Example of an alternative mathematical model

In this section a simple experiment is worked out to show how large an effect a change in the adjustment mechanism can have on a quasi geostrophic normal mode and how complex the effect is. It also serves to illustrate how small an amount of information is required to specify the adjustment process, only two conditions are required in the case illustrated. This suggests that a parametrization could be constructed by imposing a small number of rules based on observed atmospheric behaviour.

Consider the two layer model as before but write the equations as follows; on an f plane:

$$\frac{\partial \zeta_1}{\partial t} + u_1 \cdot \nabla(\zeta_1 + f) + A = 0$$

$$\frac{\partial \zeta_2}{\partial t} + u_2 \cdot \nabla(\zeta_2 + f) + B = 0 \qquad (7)$$

$$\frac{\partial \bar{T}_1}{\partial t} + u_1 \cdot \nabla \bar{T}_1 + C = 0$$

$$\frac{\partial \bar{T}_2}{\partial t} + u_2 \cdot \nabla \bar{T}_2 + D = 0$$

$$\frac{\partial p_*}{\partial t} + E = 0$$

$$\nabla^2(R\alpha_2 T_2) + \nabla \cdot (R\bar{T}_2 \nabla \ln p_*) = f\zeta_2 \quad , \quad \nabla \times \underline{u} = \zeta, \quad \nabla \cdot \underline{u} = 0$$

$$\nabla^2(R\alpha_1 T_2 + R\alpha_0 \bar{T}_1) + \nabla \cdot (R\bar{T}_1 \nabla \ln p_*) = f\zeta_1 \quad , \quad \alpha_0 = \tfrac{1}{2}\ln \sigma_2/\sigma_1 \quad , \quad \alpha_1 = \tfrac{1}{2}\ln \sigma_2/\sigma_1 + \ln \sigma_1/\sigma_2 \quad , \quad \alpha_2 = \ln \sigma_1/\sigma_2$$

(7) describes the evolution of the geostrophic flow under geostrophic advection with all the other terms in the equations left undefined. The geostrophic constraints remove two of the five arbitrary terms.

For illustration we construct the adjustment terms empirically from two approximately observed forecasting rules.

i) $A + B = 0$

This states that the vertical mean divergence is approximately zero, since the main term in A and B is the divergence.

ii) $E = e(C + D)$ (8)

E may depend on horizontal scale but is otherwise constant. This states that pressure rises in a region of descending air and vice versa. The main terms in C and D are the vertical velocity.

The linearised system analogous to (5) then becomes

$$\frac{d}{k}(iv_1) = -U_1 iv_1 + A$$

$$\frac{d}{k}(iv_2) = -U_2 iv_2 - A$$

$$\frac{d}{k}(\bar{T}_1) = -U_1 \bar{T}_1 + \frac{1}{k} iv_1 \frac{\partial \bar{T}_{m1}}{\partial y} + C \qquad (9)$$

$$\frac{d}{k}(\bar{T}_2) = -U_2 \bar{T}_2 + \frac{1}{k} iv_2 \frac{\partial \bar{T}_{m2}}{\partial y} + D$$

$$\frac{d}{k}(p_*) = e(C + D) \quad , \quad iv_2 = -\frac{Rk}{f}(\alpha_2 T_2 + T_{m2} p_*/p_0)$$

$$iv_1 = -Rk/f\,(\alpha_1 \bar{T}_2 + \alpha_0 \bar{T}_1 + T_{m1} p_*/p_0)$$

Use of the geostrophic condition will reduce the seven normal modes to three. Since there are only winds at two levels there can only be two geostrophic modes. There are three variables defining the height fields so that one degree of freedom should be removed from them to obtain the two geostrophic modes. The results quoted will be for a basic state with $\partial \bar{T}_m/\partial y$ constant, so that it is reasonable to make the restriction $\bar{T}_1 = \bar{T}_2$. The resulting system will then have two normal modes. There are four unknown quantities in the equations: A,C,D,E. Three of the four are eliminated by the geostrophic constraint and specifying $\bar{T}_1 = \bar{T}_2$, leaving one as a free parameter. The difference between this analysis and one of the primitive equations is that conditions (8) above are used instead of specifying two of the terms in the equations.

After some algebra the normal mode condition becomes

$$\begin{vmatrix} \alpha(\lambda_0+\lambda_1+\lambda_2)+k(U_1(\lambda_0+\lambda_1)+U_2) & \frac{\lambda}{\rho_0}(\bar{T}_{m_1}+\bar{T}_{m_2})+\frac{k}{\rho_0}(U_1\bar{T}_{m_1}+U_2\bar{T}_{m_2}) \\ 2\frac{e\lambda}{k}+(U_1+U_2)+\frac{k}{f}\frac{\partial \bar{T}_m}{\partial y}(\lambda_1+\lambda_0) & -\lambda/k+\frac{R\bar{T}_{m_1}}{f\rho_0}\frac{\partial \bar{T}_{m_1}}{\partial y} \end{vmatrix} = 0 \qquad (10)$$

To compare these normal modes with neutral quasi geostrophic modes from the primitive equation analysis, we set

$$\frac{\partial \bar{T}_m}{\partial y} = -10^{-5}\ ^\circ K m^{-1}, \quad f = 10^{-4}\ s^{-1}, \quad \bar{T}_{m_1} = 220^\circ K,$$

$$\bar{T}_{m_2} = 260^\circ K, \quad \rho_0 = 1000\ mb, \quad U_1 = 39.8\ ms^{-1}, \quad U_2 = 8.27\ ms^{-1}$$

Then (10) reduces to

$$(1.675 + .96e)(\lambda/k)^2 + (78.04 + 21.82e)\lambda/k + 491.1 = 0 \qquad (11)$$

For $e = 0$ this gives $\lambda/k = -39.1$ or -7.5, $e = 0$ means that there is no mechanism for baroclinic instability since the coupling through the

ρ_x field cannot operate.

$c = 1/2$ gives $\omega/k = -34.7$ or -6.6

The figures for the primitive equation model in F are $\omega/k = 39, 25$ and 9 ms^{-1} for $2\pi/k = 400$ km and 32, 30 and 14 ms^{-1} for $2\pi/k = 1200$ km. A fairly simple calculation shows that (11) has real solutions for all real values of c, so that even if c depends on k we cannot obtain unstable modes for this velocity profile.

It is not worth pursuing this analysis in any more detail since assumptions (8) were purely illustrative. Assumption (i) is not sufficiently realistic to allow synoptic developments. It is clear that the effects of the assumptions on the quasi geostrophic mode are indirect and complex.

2.4 Programme for developing alternative models

While the preceding sections illustrate the potential consequences of unrealistic representation of the geostrophic adjustment process, they do not constitute a proof that anything is wrong with it in present models, not do they indicate what could be done about it. Such a proof would require very detailed diagnostic studies, which it is not at all clear how to carry out. The standard theory is linearised and real atmospheric data is not a single spherical harmonic. However, work in this direction should be attempted.

The rest of this note assumes that there is something wrong and sets out an alternative strategy for constructing a forecast model. If better results could be obtained by doing this it would furnish an indirect proof that there is a fault in the adjustment process. These models only attempt to predict the geostrophic flow. In order to achieve the predicted geostrophic flow a large and organised ageostrophic circulation is required, it is in no sense neglected. However, it is not output directly. Some of its characteristics could be deduced if required.

These models have three aims. The first is to help understanding of atmospheric dynamics. The effects of changing the adjustment mechanism on a

forecast could give important clues as to what determines real atmospheric behaviour. The second aim is to provide more accurate forecasts at the beginning of an integration. Empirical forecasting rules have used observed relationships between, for instance, vorticity and thermal advection and synoptic development. Some of these relationships are studied in the next section. It should always be possible to ensure that the forecast starts off in the right direction, that depressions in favoured development areas deepen and so on. In primitive equation models the start of a forecast is often contaminated by initialisation and 'settling-down' problems. By building these forecasting rules into a parametrization and by localising the effects to avoid any data errors contaminating the whole area it should be possible to at least start in the right direction.

The third aim is to see if, by representing the adjustment process more realistically, it is possible to produce forecasts for longer periods than by current primitive equation models. It is not at all clear whether this is possible but it should at least be attempted.

3. Comparison of observed changes with terms in the equations of motion

The data used for this part of the study is taken from tapes supplied by NCAR and is the same as that used for the forecast intercomparison study of Baumhefner and Downey (1978). Only quantities calculated from the geostrophic flow are used here, so that only the height fields of the data sets are involved. The data includes heights of six pressure surfaces on a $2\frac{1}{2}^{\circ}$ by $2\frac{1}{2}^{\circ}$ grid. These were interpolated in the vertical to five layers: 900, 700, 500, 300 and 100 mb. The geostrophic vorticity was calculated for each of these levels, and this was then interpolated onto the quasi-uniform grid used by the finite element models (Cullen and Hall (1979)). The height fields were then recovered by solving the reverse balance equation. In low latitudes an answer was obtained by keeping f constant south of 30°N, but the resulting fields have no physical meaning.

The data are available at 12 hour intervals and the diagrams in this note cover the 24 hour period from 12 Z on 12 December 1972. An attempt is made to match difference fields over 12 hour periods with particular terms of the

equations of motion calculated from the data sets at the beginning and end. These terms will only include the contributions from the geostrophic flow.

The first set of diagrams compares the changes in the vertical mean geostrophic vorticity with the vertically meaned vorticity advection term. Figures 1 and 2 show the difference fields of mean vorticity over the two 12 hour periods and figures 3 to 5 the mean vorticity advection at the start, middle and end of the 24 hours. Thus we compare figure 1 with a mean of figures 3 and 4 and figure 2 with a mean of figures 4 and 5.

It is immediately seen from figures 3 and 4 that the changes in the advection term over 12 hours are too large for the average of the two fields to be meaningful. Thus a quantitative comparison is not possible, nor could it be without increased data coverage in time which is not available. The dominant wavenumber in the observed difference field is about 15, which is much higher than the dominant wavenumber in the observed height fields (about 6). Even so, this wavenumber should be adequately represented by current large forecasting models. The ECMWF model, for instance, will have 12 grid-points for this wavelength.

Inspection of the figures shows that, for the smaller features, there seems to be a close relation between the difference field and an intermediate chart between the two advection fields. However, such large-scale structure as there is does not seem to correspond. This is consistent with the theory behind the equivalent barotropic model, and with the rough rule that for small scales (ie $k^2\phi_0 > f^2$ where ϕ_0 is 10^5 gpm) the vertical mean divergence is small compared with the maximum divergence. The fields south of 30°N should be ignored.

The second set of diagrams compares the 900 mb height changes with the mean vertical motion in the layer 900 to 300 mb. This comparison would more properly have been made with the PMSL field but this field was not retained. The mean vertical motion was calculated from the difference between the temperature changes at 800, 600 and 400 mb due to thermal advection and those implied by

differential vorticity advection. The dominant term in the temperature equation which can balance this difference is the adiabatic term. The difference fields are shown in figs 6 and 7 and the implied vertical motion fields in figs 8 to 10.

As with the vorticity advection field, the changes in the implied vertical motion over 12 hours are too large for a quantitative comparison to be made. There is a close qualitative match between the implied vertical motion and the two sets of observed 900 mb changes. The very large scale changes of 900 mb height do not match, but these may not be realistic in any case because of the way in which the fields were derived from the reverse balance equation. There also seem to be differences of magnitude, particularly where the 900 mb height increases over the period. Examples are at 50N 60W in fig 6 where the observed change is much less that that implied by figs 8 and 9 and at 55N 20W in fig 7 where the observed changes are much greater.

Figs 11 to 13 give the actual 900 mb height charts at the three times. The position 50N 60W is anticyclonic and 55N 20W is cyclonic. The diagnostics shown here are consistent with the idea that the surface pressure changes depend for their sign on the implied vertical motion but their magnitude depends also on the local absolute vorticity. The good qualitative match suggests also that the initial data should be good enough to predict whether each anticyclone or depression should intensify or weaken over the next 12 or 24 hours.

4. Results obtained using a parametrization scheme to represent the adjustment process

4.1 Principles of construction

The scheme described here is one of many that have been investigated and should not be regarded as definitive. As discussed in section 2.4, it is designed to produce at least initially correct pressure tendencies and mean height changes. Success of the scheme in producing a good forecast beyond about 12 hours will depend on a correct forecast of such parameters as the mean vorticity advection. Since this behaves like $\nabla\bar{\phi} \cdot \nabla(\nabla^2\bar{\phi})$, involving

four derivatives, it is very much harder to forecast it correctly than to forecast the height field itself. One would therefore expect a very limited period of predictability. The situation may not be as bad as this, however. Any formulation of the equations will imply the existence of particular normal modes as discussed in section 2. Once the forecast field has become dominated by these modes a fairly stable evolution should follow. The rapid initial error growth implied by the degradation of the vorticity advection fields should then level out. However, successful forward integration for more than a few hours will certainly require conservation of energy and perhaps other quantities by the parametrization.

The present scheme is to be regarded as a successive approximation scheme. The diagnostics in section 3 suggest that the vorticity advection is the driving mechanism for mean vorticity change for wavenumbers above about 10. The first approximation is purely advective. It uses the mean vorticity advection to predict the changes, subject to three constraints. The first is that the propagation of disturbances is two dimensional, so that the mean vorticity advection is used to calculate a steering velocity which is used to advect the fields at all levels. The second constraint is that the changes should be locally determined. This avoids making unnecessary errors in areas where nothing is happening and is consistent with the idea that adjustment is not carried out by large scale wave motions propagating globally, but by local small scale processes. The third constraint is that the relative adjustment of height and wind fields required is energetically consistent.

For the second approximation we use properties of the secondary circulation. In order to achieve the two dimensional propagation a large divergence field is required to compensate for the differential advection of vorticity in the vertical. This implies a vertical motion field. The observed correlation between mean divergence, surface pressure tendencies and vertical motion is then used to recalculate the surface pressure changes. This is done in such a way that the fields at all levels propagate at the same speed in non-developing

situations. Again, the adjustments have to be energetically consistent. This constraint is more complicated to apply now that development is included and the system advection velocity produced will be different from that obtained in the first approximation.

4.2 Advective approximation

The starting point for this is the equivalent barotropic model. This stage of the calculation only attempts tc advect systems rather than develop them, and equivalent barotropic theory has performed quite well at this.

The vertically integrated vorticity equation is

$$\frac{\partial \overline{\zeta}}{\partial t} + \overline{u.\nabla(\zeta+f)} + \overline{(\zeta+f)D} + \overline{\dot{\sigma}\frac{\partial \zeta}{\partial \sigma}} = 0$$

Study of this equation shows that the $\overline{u.\nabla(\zeta+f)}$ term drives the motion of the mean vorticity field and the divergence term reduces the speed of very large scale patterns, where the winds tend to adjust to the heights.

We seek a parametrization for the divergence and vertical advection terms which is defined locally, since the physical justification for it is that adjustment is carried out in small regions of the atmosphere and not by large scale waves. This will also remove probably unwanted remote effects. The work of Lambert and Merilees (1978) indicates that primitive equation models produce unrealistically large changes in the long waves. The harmonic dials in that paper show that the real changes are very small.

To achieve locally determined height changes it is necessary to advect the height fields rather than the wind or vorticity fields. Otherwise the geostrophically implied height changes will be non-local. The geostrophic wind cannot advect the height field so an extra component has to be added to it. In order to calculate this component it is easiest to consider the temperature changes. If these are not produced by advection they must be produced by vertical motion, for we are only considering dynamical effects. It is supposed that large scale overturning motions are prohibited, so the vertical motions are restricted in magnitude. The restriction we impose is that the changes produced

by vertical motion should not be greater than those which would be produced by a wind perpendicular to the contours of the same magnitude as the mean wind. In order to implement a Lagrangian method we wish to represent the changes as advection by some wind. We therefore parametrize the vorticity advection by rotating the mean wind through an angle α less than $\pi/2$ so as to imply vorticity changes of the correct magnitude.

The angle of rotation α must be determined by the local value of $\overline{u \cdot \nabla(\zeta+f)}$. This must be converted into a dimensionless angle through which to rotate the wind $\bar{u}$. An increment X to the geostrophic vorticity implies an increment $\nabla^{-2}(fX)$ to the height field. If the field is a single spherical harmonic then this increment is $-fX/k^2$ where k is the total wavenumber. To get a locally determined increment we calculate a local wavenumber k from the relationship

$$X_0\left\{\tfrac{1}{8}k^2\Delta x^2 + O(k\Delta x)^4\right\} = X_0 - \left(\tfrac{1}{2}X_0 + \tfrac{1}{2}\bar{X}\right) \qquad (12)$$

where k^2 is the local wavenumber of a field X, Δx is the grid-length, X_0 is the local value of X and $\bar{X}$ is the average value at the adjacent points (five or six on this grid). The particular form (12) is used because the average $\tfrac{1}{2}X_0 + \tfrac{1}{2}\bar{X}$ is calculated in any case as part of the finite element algorithm.

To satisfy energy consistency we assume the estimates

$$\frac{\partial \bar{\zeta}}{\partial t} + \overline{u \cdot \nabla(\zeta+f)} + X = 0$$

and

$$\frac{\partial \bar{\phi}}{\partial t} + \bar{u} \cdot \nabla\bar{\phi} + Y = \frac{\partial \bar{\phi}}{\partial t} + Y = 0 \qquad (13)$$

and require that

$$\frac{\partial}{\partial t} f\bar{\zeta} = -\frac{\partial}{\partial t} k^2\bar{\phi}$$

and that the change in kinetic energy implied by X is equal to the change in available potential energy implied by Y.

The kinetic energy density change will be of order

$$u\delta u = u\delta(\zeta/k) \sim \frac{uX}{k}$$

and the potential energy density change of order $\delta\phi = Y$

The consistent estimate for $\frac{\partial\bar{\Phi}}{\partial t}$ is therefore

$$-\frac{f}{k^2}\left(u.\overline{\nabla(\zeta+f)}\right).\frac{1}{1+f/ku} \qquad (14)$$

subject to the maximum value of $|u||\nabla\phi| = fu^2$

It is this part of the scheme that requires most further work. Because most of the adjustment occurs in limited 'shock-like' regions where energy can be dissipated into gravity waves, it is possible that the energy constraint is not the right one to use.

4.3 Numerical implementation of system advection

This scheme is implemented by using a Lagrangian representation of the height field. The field is defined by marker particles which carry values of the height at the chosen model levels. For the system advection stage these height values are held constant and the particle positions moved with the system velocity $\tilde{u}$. This prevents loss of information during the forecast. To avoid an extremely expensive and inaccurate numerical scheme, the system velocity is calculated on a fixed Eulerian grid using heights calculated by a high order interpolation scheme from the five nearest marker particles. The winds are then interpolated to the marker particle positions and used to move the particles. The effect of this is to smooth the implied wind field somewhat but the particle positions need never be interfered with so that the height information is retained through the forecast. The only need to rearrange particles would be if particles were swept through the boundary. Since the boundary is at the equator and no serious attempt is made to predict low latitude systems it is unlikely that many particles will be lost.

The Eulerian grid used in the experiments is the quasi regular grid used for the diagnostic calculations in section 3. All quantities are calculated using the finite element algorithms from Cullen and Hall (1979). The method is expensive, $O(N^2)$ for N particles, because of the need to find the nearect

five marker particles to each point of the fixed grid. Some such expense is unavoidable if the particles are never re-interpolated and can move in a completely general way. There is scope for developing more efficient search algorithms.

4.5 Results using system advection

12 and 24 hour forecasts of surface pressure and 900-500 mb thickness are shown in figs 14-15 and figs 21-22. Actual values for the initial time and the two forecast times are shown in figs 11 to 13 and 18 to 20. Implied surface pressure values are deduced from the 900 mb heights, which are carried by the model, using the same algorithm for forecast and verification fields. Verification is difficult because only the advective terms have so far been included and it is difficult to distinguish changes due to system advection from changes due to development.

The surface pressure 12 hour forecast moves the pressure systems in the right direction but too rapidly in most cases. No changes in central pressure can be predicted by this part of the scheme so it is difficult to evaluate the forecast of the rapidly developing systems. Ly 24 hours the excessive movement is serious between 150°W and 150°E at 60°N.

The thickness forecast should be a more reliable guide to the performance of this part of the scheme since the second approximation changes the surface pressure forecast more than the thickness. However no changes due to physical effects will be forecast.

The changes between 60°E and 60°W are mostly correctly forecast except that excessive changes are produced near 30°W 60°N. By 24 hours the changes between 150 and 180W are also excessive. Elsewhere the phases of most features are correct and the amplitudes much closer to reality than might be expected from a purely advective scheme.

It is probably unwise to conclude too much from an assessment of only part of the scheme. However, most of the thickness changes have been correctly forecast and it is therefore reasonable to move to a second approximation which

uses a different means of predicting surface pressure but similar techniques for predicting thickness.

4.6 Representation of the development terms

This part of the parametrization is based on the observation that surface pressure rises in regions of descending air and vice versa. The vertical velocity can be deduced from the advective part of the parametrization by comparing the temperature change produced by the system advection with that produced by thermal advection. The mathematics of this is set out in Hoskins et al (1978). Assume that

$$\frac{\partial \phi_s}{\partial t} = \bar{\Sigma} \alpha_i \omega_i \qquad (15)$$

where the ω_i are the implied pressure vertical velocities, ϕ_s is the 1000 mb geopotential and the α_i are to be determined. The mathematical analysis shows that (15) will predict the changes in ϕ_s due to advection as well as to development. This is because $u_s \cdot \nabla T = - u_T \cdot \nabla \phi_s$ if the surface and thermal winds u_s and u_T are geostrophic. Therefore the α_i can be determined by requiring that (15) reduces to

$$\frac{\partial \phi_s}{\partial t} = - \tilde{u} \cdot \nabla \phi_s$$

in non-developing situations. As in section 4.3 we must now write out the equations of the approximation and ensure energy consistency. The required non-development condition can then be imposed. First of all consider the simplified primitive equations in the form

$$\frac{\partial \mathcal{I}}{\partial t} + u \cdot \nabla (\mathcal{I} + f) + f \mathcal{D} = 0 \qquad (16)$$

$$\frac{\partial}{\partial t}\left(\frac{\partial \phi}{\partial p}\right) + u \cdot \nabla \left(\frac{\partial \phi}{\partial p}\right) + w = 0 \qquad (17)$$

$$\frac{\partial \phi_s}{\partial t} + \phi_0 \bar{\mathcal{D}} = 0 \qquad (18)$$

$$\bar{\mathcal{D}} = \bar{\Sigma} \beta_i w_i \qquad (19)$$

where the overbar is a vertical mean, w is related to the vertical motion, the β_i depend on pressure and ϕ_s is the geopotential at 1000 mb. Many

terms have been neglected, and (19) is a weighted integral of the continuity equation. The feature of the primitive equations which ensures a balanced conversion between potential and kinetic energy is retained because of the relation between $\bar{D}$ and w and the form of the divergence term in the vorticity equation. As in section 4.3 we form a local approximation to (16) using a local wavenumber k to convert vorticity increments to height increments. Thus

$$\frac{\partial \bar{\psi}}{\partial t} - \frac{f}{k^2}\left(u.\overline{\nabla(J+f)}\right) - f^2/k^2\,\bar{D} = 0 \qquad (20)$$

$$\frac{\partial}{\partial t}(\bar{\phi} - \phi_s) + \alpha\,\overline{u.\nabla\left(\frac{\partial \phi}{\partial p}\right)} + \alpha\bar{\omega} = 0 \qquad (21)$$

$$\frac{\partial}{\partial t}\phi_s + \phi_0 \bar{D} = 0 \qquad (22)$$

(21) is a weighted mean of (17) over the levels, the weights are selected so that the time derivative term takes the form shown. To calculate the α_i and to define the weights in the continuity relationship (19) consider the case where the thermal gradient is parallel at all levels so that

$$u.\nabla\frac{\partial \phi}{\partial p} = u_s.\nabla\frac{\partial \phi}{\partial p} \qquad (23)$$

In this case the second term of (21) must become $u_s.\nabla(\bar{\phi} - \phi_s)$. This is equal to $-(\bar{u} - u_s).\nabla\phi_s = -\bar{u}.\nabla\phi_s$. If we suppose a non-developing situation to be defined by (23) and $\frac{\partial}{\partial t}(\bar{\phi} - \phi_s) = 0$, then (22) must become

$$\frac{\partial}{\partial t}\phi_s + \bar{u}.\nabla\phi_s = 0$$

and so $\phi_0\bar{D} = \bar{u}.\nabla\phi_s$ and $\alpha\bar{\omega} = \phi_0\bar{D}$. The last equality thus defines the weights in (19), and so in general we can write

$$\frac{\partial}{\partial t}(\bar{\phi} - \phi_s) + \alpha\,\overline{u.\nabla\left(\frac{\partial \phi}{\partial p}\right)} + \phi_0\bar{D} = 0 \qquad (24)$$

In a simple case the relationship $\overline{d\omega} = \phi_0 \bar{D}$ is consistent with the standard continuity equation $D = \partial\omega/\partial p$.

Define $\overline{u.\nabla(\zeta+f)} \equiv A$, $\overline{\alpha u.\nabla(\partial\phi/\partial p)} \equiv B$. These are both known quantities.

Then from (20) and (22)

$$\frac{\partial}{\partial t}(\bar{\phi} - \phi_s) - \frac{fA}{k^2} - (f^2/k^2 + \phi_0)\bar{D} = 0$$

and from (24)

$$\frac{\partial}{\partial t}(\bar{\phi} - \phi_s) + B + \phi_0 \bar{D} = 0$$

giving

$$\frac{\partial}{\partial t}(\bar{\phi} - \phi_s) = \frac{\phi_0(B + fA/k^2)}{2\phi_0 + f^2/k^2} - B \qquad (25)$$

$$\bar{D} = -\frac{B + fA/k^2}{2\phi_0 + f^2/k^2} \qquad (26)$$

To implement the scheme we use (25) to calculate a steering velocity $\tilde{u}$ such that

$$-\tilde{u}.\nabla(\bar{\phi} - \phi_s) = \partial/\partial t(\bar{\phi} - \phi_s) \qquad (27)$$

subject to $|\tilde{u}| = |\bar{u} - u_s|$

The restriction on overturning is thus enforced the same way as in section 4.3. The tendency $\partial\phi_s/\partial t$ is then equal to $\partial/\partial t(\bar{\phi} - \phi_s)$ which is

$$\frac{\partial}{\partial t}(\bar{\phi} - \phi_s) + \overline{\alpha u.\nabla(\partial\phi/\partial p)}$$

The numerical representation of this tendency is chosen to be consistent with that of the advective terms. Consider a point P on the fixed grid. The advection of the height fields by the velocity $\tilde{u}$ will give a tendency $\delta\phi_s^*$ at P calculated by interpolation from the nearest marker particles. The advection stage is then repeated using each u_i in turn in order to calculate $u_i.\nabla(\phi_{i-1} - \phi_i)$. To avoid unnecessary expense the same five marker

particles are used to determine the temperature tendency at P as were used in the main advective step. This also gives greater consistency between $u_i \cdot \nabla(\phi_{i-1} - \phi_i)$ and $\hat{u} \cdot \nabla(\phi_{i-1} - \phi_i)$ so that their difference is more accurate. These differences are proportional to the implied vertical motion and $\delta\phi_s$ is calculated from them. The difference $\delta\phi_s - \delta\phi_s^*$ at P is then the development term at P. The field of $\delta\phi_s - \delta\phi_s^*$ on the fixed grid is then interpolated to the marker particles and used to increment their values of ϕ at all levels. The temperature fields are therefore not modified at this stage. Some smoothing of the developments will result.

4.7 Forecast results using the development term

The 12 and 24 hour forecasts of surface pressure and 900-500 mb thickness are shown in figs 16-17 and 23-24. The 12 hour surface pressure forecast now captures most of the developments not present in the purely advective version. The forecast at 55N 30W and 40N 70W for instance is much better. Detailed checking of central pressures, however, shows that the changes are only correctly forecast in about half the cases. The errors mostly take the form of excessive changes to the initial values and production of too much small-scale detail, for instance over the Atlantic. However, the model is reluctant to get rid of features, for instance the depression at 65N 10W. There is a problem at the North Pole due to technical difficulties in constructing a consistent scheme there.

At 24 hours the reluctance to weaken features has led to serious errors. By this time the purely advective forecast in fig 15 is more realistic. It was found during other experiments that even attainment of results as good as fig 17 required use of the energy argument of the previous section.

The thickness forecasts are similar to those produced by the advective scheme as expected. The excessive distortions produced at 12 hours near 60N 30W and at 24 hours near 50N 160E are reduced in this forecast. The amplitude of the developing ridge at 70W is also better forecast especially at 24 hours. However, there are other errors which are common to both.

These results suggest that the representation of surface pressure changes used here is able to improve the 12 hour forecast substantially as compared to a purely advective prediction. However, after this time the results diverge. This is probably not surprising at the current state of development of the scheme.

5. Discussion

The diagnostic results in section 3 suggest that available data sets contain sufficient information to make a qualitative prediction of the development of systems within the next 12 hours in most cases. There are some cases, perhaps 20 percent of the systems, where the information would have been misleading. The experiments described in section 4 can be regarded as an attempt to convert this into a quantitative forecasting tool. Viewed in this way the results show some promise at 12 hours, but very little at 24 hours. In order to improve the 24 hour forecast some more information must be included in the scheme. This will certainly include physical effects. However, the results indicate a tendency to amplify features of the wrong scale and structure and suggest that a more selective representation of the development process is required. The representation in a conventional model is more selective, and this explains why reasonable results can be obtained for long integrations. It is necessary to make the parametrized model more selective while enforcing the extra constraints which it is postulated are not enforced in the primitive equation models. This in particular includes the restriction of overturning motions. Future development will have to include deriving appropriate consistency requirements from the primitive equations and applying them to the parametrized model in a similar way to the use of the energy constraint applied in section 4.6. The result will be a constrained form of the primitive equations, which is what is desired. It is difficult to see how this aim can be achieved by directly modifying the values of vertical velocity in the primitive equations because the model then departs unrealistically from geostrophic balance.

References

Baumhefner, D P, Downey, P. 1978 'Forecast intercomparisons from three numerical weather prediction models', Mon Weath Rev 106, pp 1245-1279.

Blumen, W. 1972 'Geostrophic adjustment', Rev Geoph Space Phys, 10, pp 485-528.

Cullen, M J P. 1979 'A study of some possible effects of the geostrophic adjustment mechanism on forecasts by primitive equation models', UK Met Office MRCP 464.

Cullen, M J P, Hall, C D. 1979 'Forecast and general circulation results using finite element models', Q J Roy Met Soc 105, pp 571-592.

Cullen, M J P, Prince, J W, Radford, A M, Roskilly, D R. 1981 Forecast intercomparisons from three numerical weather prediction models from the UK Meteorological Office', submitted to Monthly Weather Review.

Findlater, J. 1980 'A preliminary report on the subjective comparison of medium range forecasts produced by ECMWF and the Meteorological Office', Met O 11 Technical Note no 137.

Foreman, S J. 1978 'Investigations of a two level linear baroclinic instability model', Met O 11 Technical Note no 114.

Gadd, A J. 1980 'The GARP Basic Data Set project: the experiment using GFDL analyses', GARP WGNE report no 20.

Hoskins, B J, Simmons, A J. 1975 'A multi-layer spectral model and the semi-implicit method', Q J Roy Met Soc 101, pp 637-656.

Hoskins, B J, Draghici, I, Davies, H C. 1978 'A new look at the ω equation', Q J Roy Met Soc, 104, pp 31-38.

Kasahara, A. 1979 'Towards achieving the goal of atmospheric scientists - understanding our atmosphere', Atmospheric Technology (NCAR), 11, pp 4-10.

Lambert, S J, Merilees, P E. 1978 'A study of planetary wave errors in a spectral numerical weather prediction model', Atmosphere-Ocean 16, pp 197-211.

List of figures

Fig 1 Difference field of the vertical mean geostrophic vorticity, 00Z 13.12.72 minus 12Z 12.12.72. Negative values are shaded.

Fig 2 As fig 1, 12Z 13.12.72 minus 00Z 13.12.72.

Fig 3 Vertical mean advection of geostrophic vorticity by the geostrophic wind at 12Z 12.12.72. Implied negative vorticity tendencies are shaded.

Fig 4 As fig 3 at 00Z 13.12.72.

Fig 5 As fig 4 at 12Z 13.12.72.

Fig 6 Difference field of surface pressure 00Z 13.12.72 minus 12Z 12.12.72. Negative values are shaded.

Fig 7 As fig 6, 12Z 13.12.72 minus 00Z 13.12.72.

Fig 8 Vertical motion between 900 and 300 mb implied by vertical difference of vorticity advection minus Laplacian of thermal advection at 12Z 12.12.72. Upward motion shaded.

Fig 9 As fig 8 for 00Z 13.12.72.

Fig 10 As fig 9 for 12Z 13.12.72.

Fig 11 Surface pressure field at 12Z 12.12.72.

Fig 12 Contour interval 4 mb at 00Z 13.12.72.

Fig 13 As fig 11 at 12Z 13.12.72.

Fig 14 As fig 11 12 hour surface pressure forecast valid 00Z 13.12.72 using advective terms only.

Fig 15 As fig 14, 24 hour forecast valid 12Z 13.12.72.

Fig 16 12 hour forecast as fig 14 using development terms also.

Fig 17 24 hour forecast as fig 16.

Fig 18 900-500 mb thickness field at 12Z 12.12.72. Contour interval 6 dm.

Fig 19 As fig 18 at 00Z 13.12.72.

Fig 20 As fig 18 at 12Z 13.12.72.

Fig 21 12 hour 900 to 500 mb thickness forecast valid 00Z 13.12.72 using advective terms only.

List of figures continued

Fig 22 24 hour forecast as fig 21.

Fig 23 12 hour forecast as fig 21 using development terms also.

Fig 24 24 hour forecast as fig 23.

Fig. 1

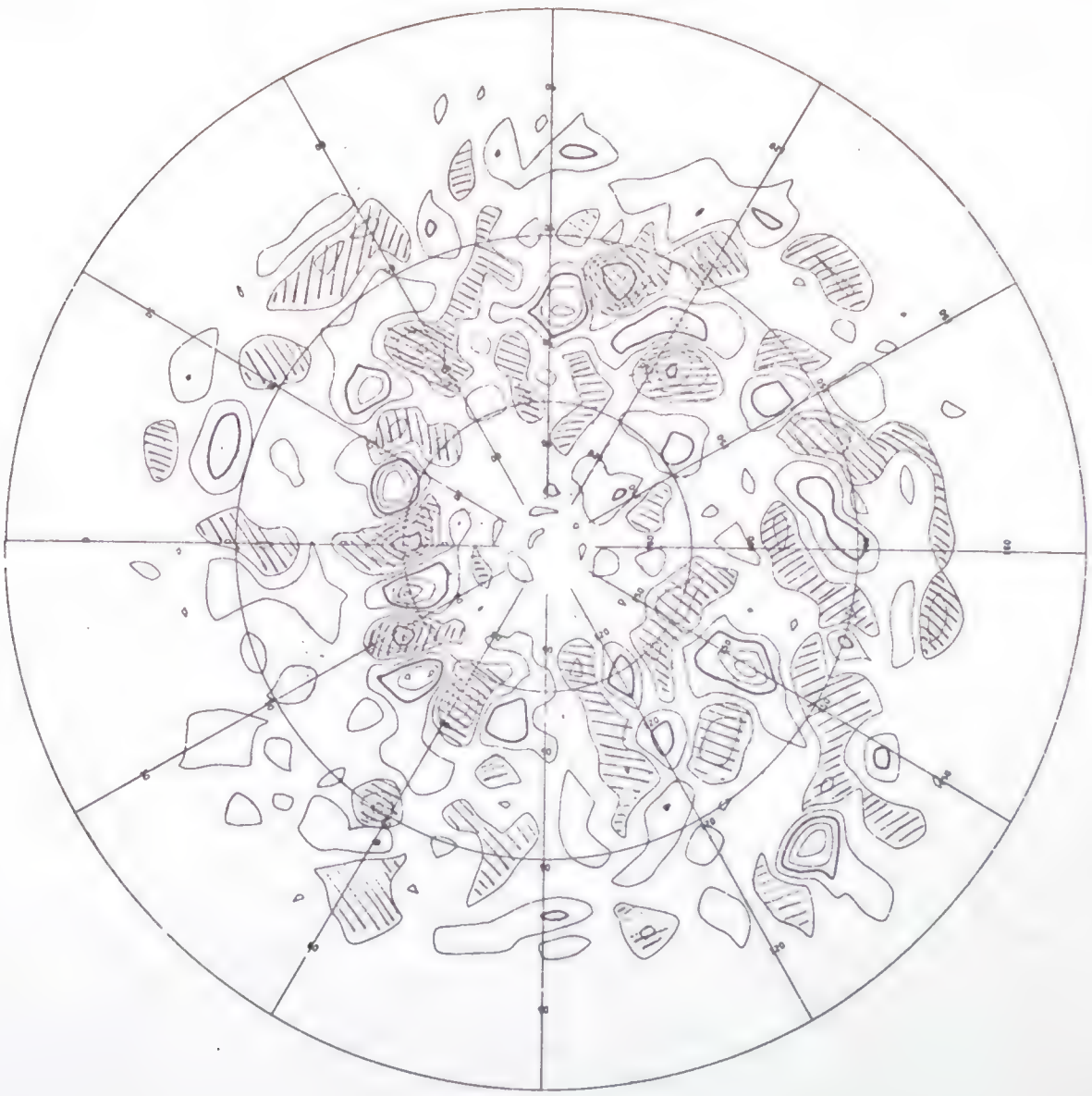

FIG. 2

FIG. 3

FIG. 5

9.51:1

FIG. 7

FIG. 8

FIG. 9

FIG. 10

FIG. 11

FIG 12.

FIG. 13

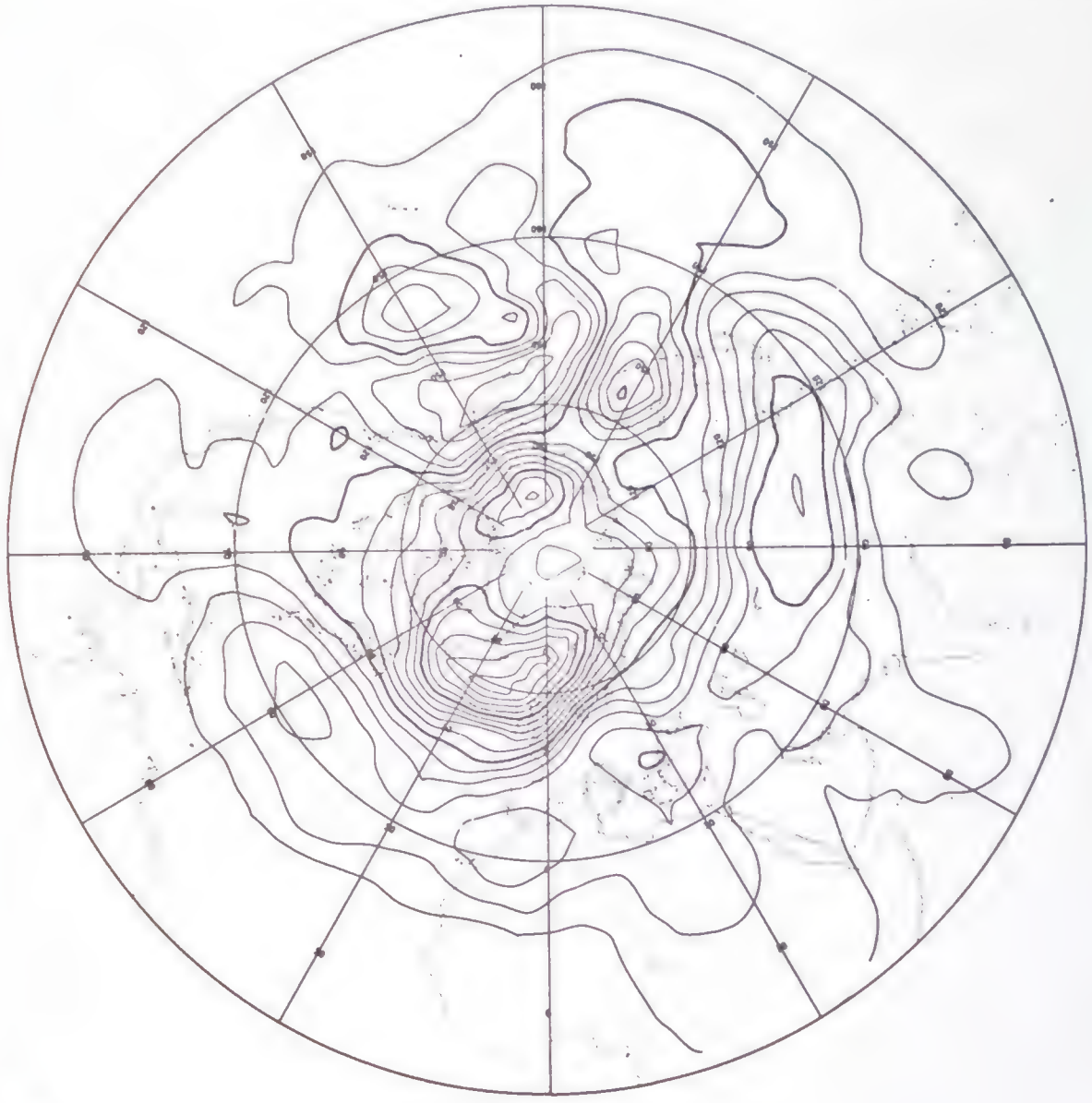

FIG. 14

Fig. 15.

FIG. 16

FIG. 18

FIG. 19

FIG. 20

FIG. 21

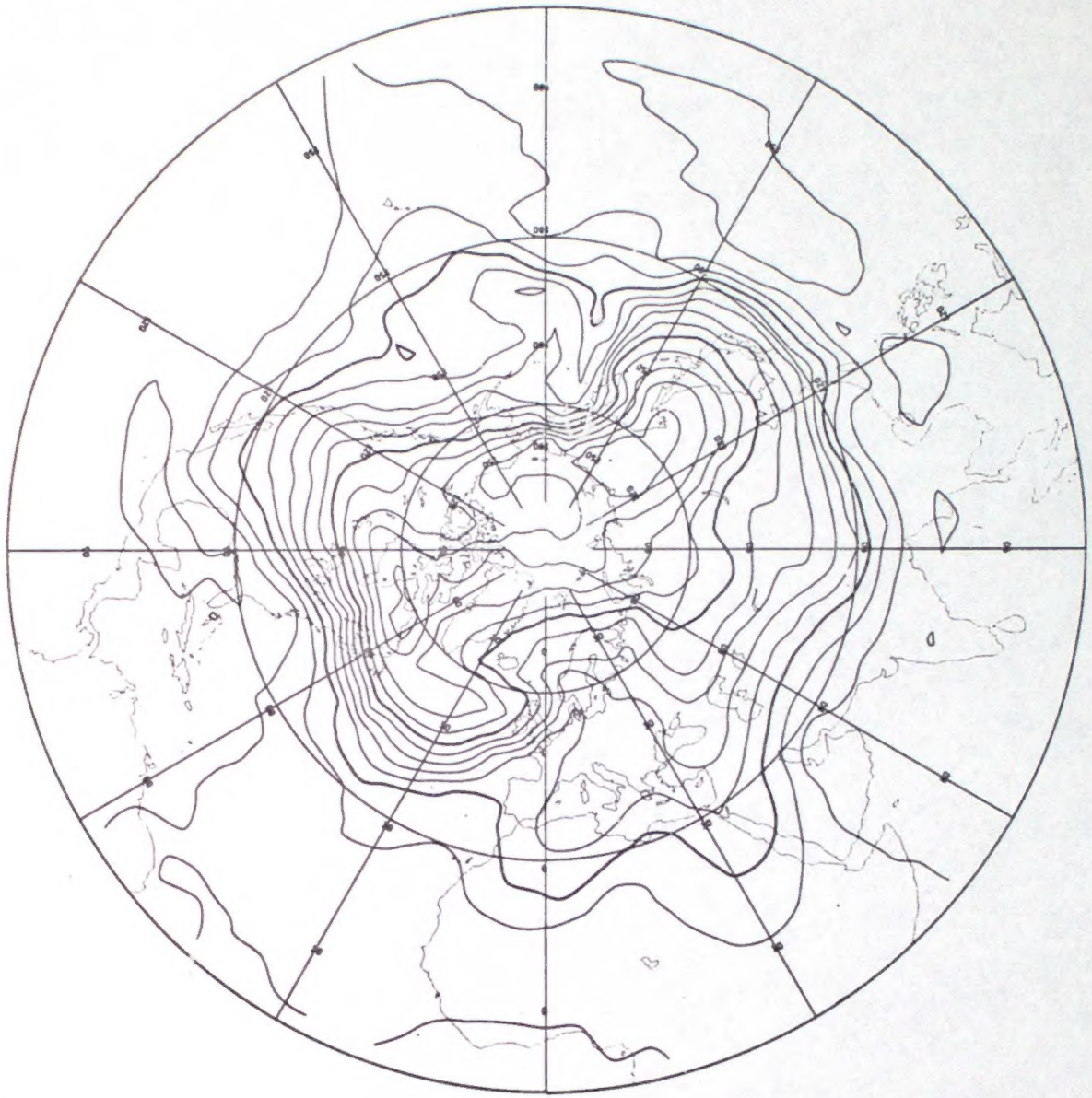

Fig. 22

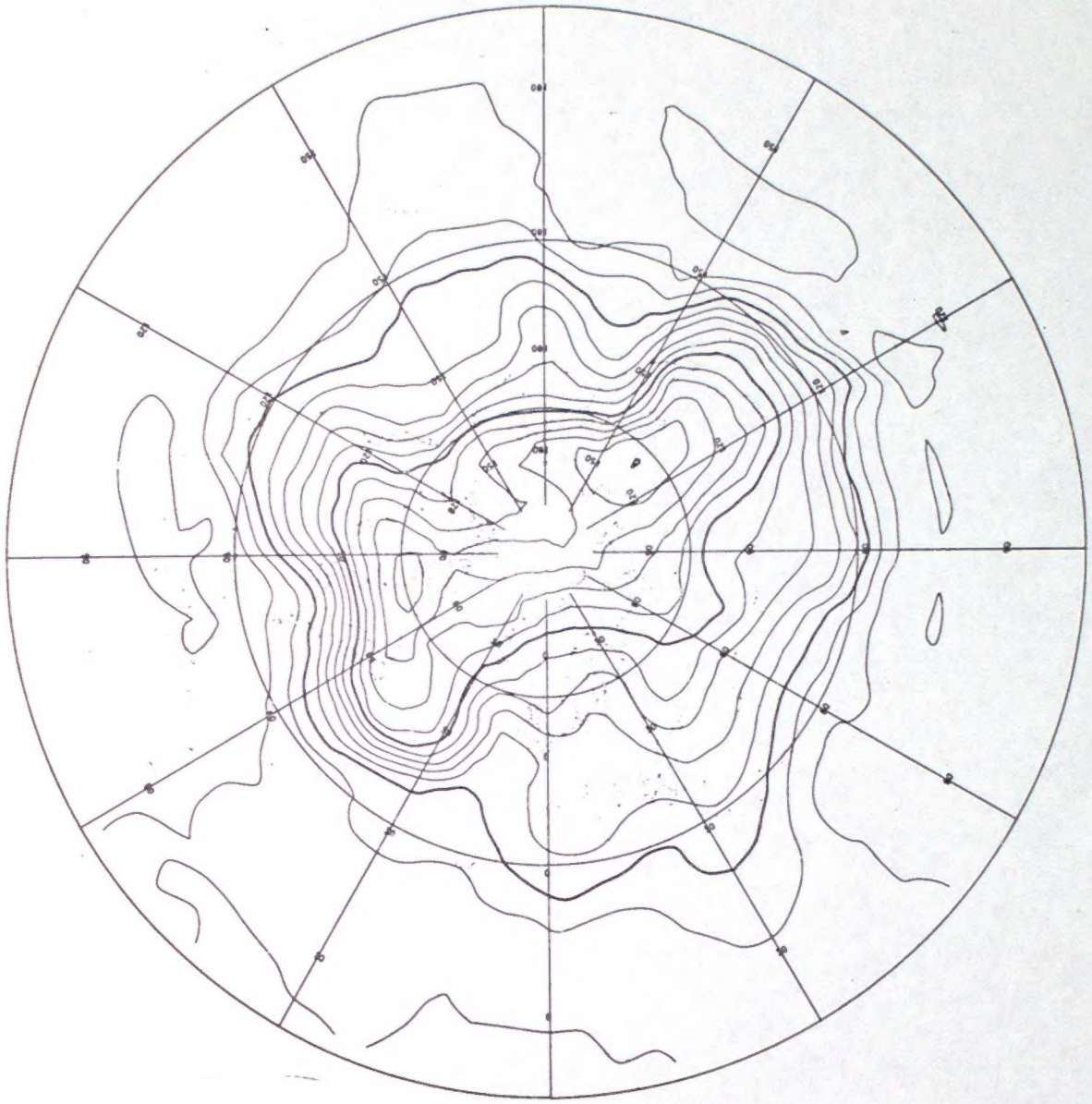

FIG. 23

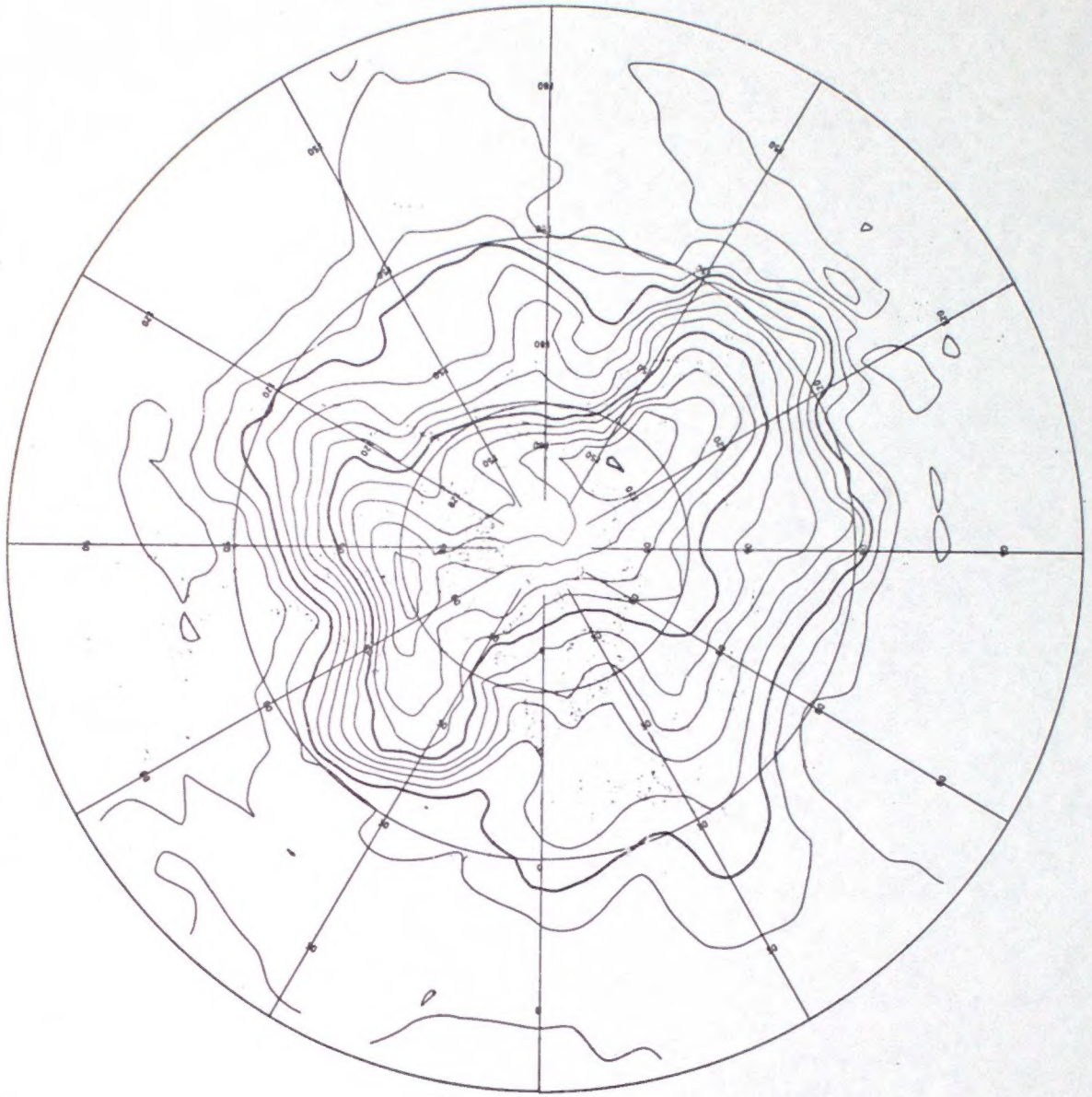

FIG. 24